Model for the structure function constant for index of refraction fluctuations in Rayleigh-Bénard turbulence

Robert A. Handler,[1,2,*] Richard J. Watkins,[3] Silvia Matt,[4] and K. P. Judd[5]

[1]*Department of Mechanical Engineering, George Mason University, Fairfax, Virginia 22030, USA*
[2]*Center for Simulation and Modeling, George Mason University, Fairfax, Virginia 22030, USA*
[3]*Micro-Photonics Laboratory, the Holcombe Department of Electrical and Computer Engineering, Center for Optical Materials Science and Engineering Technologies (COMSET), Clemson University, Clemson, South Carolina 29634, USA*
[4]*Naval Research Laboratory, Stennis Space Center, Mississippi 39529, USA*
[5]*Naval Research Laboratory, Washington, DC 20375, USA*

(Received 2 November 2023; accepted 8 April 2024; published 8 May 2024)

A model for the structure function constant associated with the index of refraction fluctuations in Rayleigh-Bénard turbulence is developed. The model is based upon the following assumptions: (1) the turbulence is homogeneous and isotropic at or near the midplane, (2) the rate of production is in balance with the rate of dissipation, (3) an inertial region exists, and (4) estimates for the rate of dissipation of temperature fluctuations and of turbulent kinetic energy can be made by assuming that the large-scale turbulence is dissipated in one eddy turnover time. From these assumptions, the dependence of the structure function on the geometry, heat flux, and the properties of the fluid is obtained. The model predicts that the normalized structure function constant is independent of the Rayleigh number. To verify the model, numerical simulations of Rayleigh-Bénard turbulence were performed using two different approaches: an in-house code based on a pseudospectral method, and a finite volume code which employs a model for the smallest scales of the turbulence. The model was found to agree with the results of the simulations, thereby lending support for the assumptions underlying the theory.

DOI: 10.1103/PhysRevFluids.9.054605

I. INTRODUCTION

Inhomogeneities in the index of refraction field resulting from turbulent temperature fluctuations are a common occurrence in both the atmosphere and hydrosphere. These fluctuations are a contributor, in addition to scattering and absorption, to the degradation of the propagation of light. One such well-known effect attributed to atmospheric turbulence is the twinkling of stars. In this case, the intensity level of the light is observed to vary in an irregular manner (scintillation). The resulting index of refraction fluctuations are frequently referred to as optical turbulence. Light fields propagating through optical turbulence suffer from a spreading effect (beyond diffraction), fluctuations in the light beam position referred to as beam wander, and irradiance variation [1]. Thus, optical turbulence imposes limits on the performance capabilities of imaging systems, sensor networks, directed-energy weapons, and laser-based communications [free space optics (FSO)]. Furthermore, insight into the interactions of light propagation through a turbulent medium using physics-based approaches may inform higher fidelity models for the prediction of optical system performance parameters. This could precipitate the development of advanced real-time adaptive

*Corresponding author: rhandler@gmu.edu

optical systems that continually adjust their performance characteristics to compensate for signal deterioration induced by evolving or degraded environmental conditions.

Field experimentation, both in the atmosphere and the water column, has provided a wealth of information and contributed to various correlations between the environmental state and optical propagation parameters [2–6]. However, experiments are often cost prohibitive, the environmental conditions are typically uncontrolled, and may only provide limited spatial information from a finite number of deployed instrumented monitoring stations. Numerical computations are proving to be a cost effective and powerful approach to simulating multiphysics phenomena whose outcomes may be used to inform and optimize experimental efforts. For this investigation, the Rayleigh-Bénard (RB) turbulent convection problem is the framework in which we study the optical properties that affect light propagation. Turbulent RB convection serves as a canonical flow model for various environmental areas of research and technological applications [7]. In addition, the model configuration has many attractive qualities for both experimental and simulation approaches such as a simple geometrical setup, well defined boundary conditions, well understood stability and transition characteristics, and rich dynamical behavior [8,9].

In light propagation studies through a turbulent medium, the magnitude of the index of refraction structure constant (C_n^2) is often reported since it provides the magnitude of the variation in the refractive index, and hence an estimate of the *strength* of the turbulence. Representative values, for horizontal propagation in the atmosphere, range from 10^{-17} m$^{-2/3}$ for weak turbulence to 10^{-13} m$^{-2/3}$ for strong turbulence [1]. A predictive model for the behavior of the index of refraction structure constant may be integrated directly into optical design expressions to estimate aperture size limits, optical element diameters, spot size resolution, and other optical system performance metrics [10].

The purpose of the current work is to determine the efficacy of determining the properties of optical turbulence, and specifically C_n^2, through the use of three-dimensional numerical simulations of Rayleigh-Bénard turbulence, which serves as a convenient model for many environmental flows driven by buoyancy. The simulations were carried out for air using both a pseudospectral method, and a finite-volume method which employs a large-eddy-simulation model of the smallest scales of turbulence. The simulations, which were carried out using identically the same fluid properties, computational domain size, and Rayleigh (Ra) numbers, were used to determine C_n^2 over an order of magnitude change in Ra. In addition, a model for C_n^2 was developed based on the scaling laws of turbulence in the inertial range of turbulent length scales. The model was found to be in good agreement with the simulations, indicating the efficacy in using numerical simulations to obtain important properties of optical turbulence, as well as a means of verifying theoretical estimates of these properties.

II. PROBLEM FORMULATION

The problem of interest, which is referred to as the Rayleigh-Bénard (RB) problem [9], is that of a fluid initially at rest in a gravitational field which is driven by a temperature difference between two parallel plates. In such a fluid, temperature differences give rise to density differences, which in turn give rise to buoyancy forces. When buoyancy forces are sufficiently strong to overcome viscous forces and thermal diffusion, fluid motion results. This problem is generally difficult to solve since the fluid cannot be considered incompressible. However, when temperature induced density differences are small compared to a reference density, the Boussinesq approximation is often employed [11]. We employ this approximation in this work.

The Boussinesq equations of motion are given by

$$\frac{D\boldsymbol{V}}{Dt} = -\rho^{-1}\nabla \mathrm{p} + \nu\nabla^2\,\mathbf{V} + \boldsymbol{f_B}, \tag{1}$$

where D/Dt is the material derivative, p is a modified pressure, ρ is a reference density, ν is the kinematic viscosity, $\boldsymbol{V} = (u, v, w)$ is the fluid velocity in the x, y, z directions respectively,

gravitational forces act in the negative y direction, and x and z denote coordinates in the horizontal plane. In addition, $\boldsymbol{f_B}$ is the buoyancy body force per unit mass given by $\boldsymbol{f_B} = g\beta\theta\hat{\boldsymbol{j}}$ where g is the gravitational acceleration, β is the coefficient of expansion of the fluid, $\theta = T - T_0$, where T is the temperature and T_0 is a reference temperature, and $\hat{\boldsymbol{j}}$ is a unit vector in the positive y direction. Consistent with the Boussinesq approximation, conservation of mass is given by

$$\nabla \cdot \boldsymbol{V} = 0, \tag{2}$$

and the temperature field is governed by

$$\frac{D\theta}{Dt} = \alpha \nabla^2 \theta, \tag{3}$$

where $\alpha = k/\rho c_p$ is the thermal diffusivity, k is the thermal conductivity, and c_p is the heat capacity at constant pressure. The above formulation leads to three nondimensional numbers: the Nusselt number, $\mathrm{Nu} = QL/k\Delta T$, the Rayleigh number, $\mathrm{Ra} = \beta g \Delta T L^3/\nu\alpha$, and the Prandtl number, $\mathrm{Pr} = \nu/\alpha$, where L is the distance between the plates which have fixed temperatures which differ by ΔT, and the vertically directed average heat flux from the bottom plate is Q. From dimensional arguments we must have $\mathrm{Nu} = F(\mathrm{Ra}, \mathrm{Pr})$, which implies that the nondimensional heat flux given by the Nusselt number depends only on the Rayleigh and Prandtl numbers.

III. NUMERICAL SIMULATIONS

A. Fluid properties, boundary conditions, and initial conditions

Rayleigh-Bénard turbulence in air was simulated by two different numerical schemes: (A) Pseudospectral methods using an in-house code, and (B) A finite-volume method which employs a large-eddy-simulation (LES) model using the open source computational fluid dynamics package OPENFOAM toolbox. It should be noted that the spectral simulations used in this work do not use turbulence models and will be referred to as direct numerical simulations (DNSs).

The same computational domain size, fluid properties, and boundary conditions were used for both spectral and OPENFOAM simulations. On the top and bottom walls of the domain, no-slip conditions were imposed on the velocity field and the walls were kept at constant temperature. Periodic boundary conditions were applied in the x and z directions.

The properties of air were chosen at 293.15 K, and are as follows: $\nu = 1.516\times10^{-5}$ m^2/s, $\alpha = 2.074\times10^{-5}$ m$^2/s$, $\beta = 3.411\times10^{-3}$ K^{-1}, and $k = 2.514\times10^{-2}$ W/(m − K). The Prandtl number, specific heat, density, and atmospheric pressure were $\mathrm{Pr} = 0.7309$, $c_p = 1007$ J/(kg − K), $\rho = 1.204$ kg/m^3, and $p_0 = 1013.25$ millibars. The computational domain dimensions were $L_x = 0.5$ m, $L_y = L = 0.1$ m, and $L_z = 0.5$ m in the x, y, and z directions respectively. In the OPENFOAM simulations, the initial velocity was set equal to zero, and the temperature field was set to its ambient value. In the spectral simulations, the initial velocity components were set equal to small random values, and the initial temperature field was chosen to be the linear conduction profile given by $T(y) = \Delta T(\frac{1}{2} - \frac{y}{L}) + T_0$ where $y = 0$ defines the center of the domain. With this initial condition for the temperature field, the Nusselt number at time $t = 0$ is $\mathrm{Nu} = 1$, since the initial heat flux at the bottom wall is $Q = -k\partial T/\partial y = k\Delta T/L$. We note that when $\mathrm{Ra} > 1708$ [9] this flow will be unstable to infinitely small disturbances, but the Rayleigh numbers in our simulations were about two to three orders of magnitude greater than this, resulting in self-sustaining turbulence.

B. Description of DNS and LES simulations

For both DNS and LES simulations, five simulations were performed for $\Delta T = 1\,^\circ$C, $2\,^\circ$C, $5\,^\circ$C, $10\,^\circ$C, and $20\,^\circ$C, which correspond to Rayleigh numbers of 1.063×10^5 to 2.126×10^6. Further details concerning the simulations are given in Table I. In all simulations, statistics were obtained from uncorrelated realizations of the velocity and temperature fields, after the flow reached a statistically steady state.

TABLE I. List of simulation parameters for spectral and finite volume simulations.

Numerical method	Temperature difference (ΔT °C)	Rayleigh number (Ra)	Grid size (x, y, z)	Time step (s)	Total simulation time (s)
Pseudospectral (DNS)	1.0	1.063×10^5	$128\times65\times128$	1.5×10^{-4}	240
	2.0	2.126×10^5	$128\times65\times128$	1.5×10^{-4}	240
	5.0	5.315×10^5	$128\times65\times128$	1.5×10^{-4}	240
	10.0	1.063×10^6	$128\times65\times128$	1.5×10^{-4}	240
	20.0	2.126×10^6	$128\times65\times128$	1.5×10^{-4}	240
Finite volume (LES)	1.0	1.063×10^5	$250\times250\times250$	1.0×10^{-2}	75
	2.0	2.126×10^5	$250\times250\times250$	1.0×10^{-2}	75
	5.0	5.315×10^5	$250\times250\times250$	1.0×10^{-2}	75
	10.0	1.063×10^6	$250\times100\times250$	variable	35
	20.0	2.126×10^6	$250\times100\times250$	variable	35

The spectral simulations, which employ Eqs. (1)–(3), were performed on the Clemson University Palmetto Cluster using an in-house pseudospectral code [12] which employs Fourier modes in the horizontal ($x-z$) plane and Chebyshev modes in the vertical (y) direction. The grid resolution was $128\times65\times128$ in the x, y, and z directions respectively, and the time step was $\Delta t = 1.5\times10^{-4}$ s. In each simulation, the Rayleigh number was fixed by choosing a temperature difference between top and bottom walls. The physical time duration for each simulation was 240 s.

The OPENFOAM, finite volume simulations were performed on Centennial, an SGI ICE XA with 1848 compute nodes, at the Army Research Laboratory, Department of Defense Supercomputing Resource Center (ARL DSRC), one of the supercomputing centers of the DoD High Performance Computing Modernization Program (HPCMP). OPENFOAM is a Navier-Stokes solver based on the finite volume method. For turbulence modeling, the large eddy simulation (LES) approach was used, where the model solves the filtered Navier-Stokes equations. The filter size is dependent on the grid spacing and the subgrid scales (SGSs) are modeled. In our setup, SGS stresses were modeled using the wall adapting local-eddy viscosity (WALE) model [13]. The grid resolution was $250\times250\times250$ in the x, y, and z directions for the runs with $\Delta T = 1\,^\circ$C, $2\,^\circ$C, $5\,^\circ$C. For the cases with higher Rayleigh number (i.e., $\Delta T = 10\,^\circ$C, $20\,^\circ$C) the grid resolution was $250\times100\times250$. The time step for these simulations was $\Delta t = 1.0\times10^{-2}$ s for the lower Ra cases and were variable for the higher Ra simulations with a criterion to keep the CFL (Courant-Fredrichs-Lewy) number less than 1 [14], a requirement for numerical stability.

It should be noted that spectral methods exhibit exponential convergence [15] and have been used with success in simulating a wide variety of turbulent flows [16]. This accounts for the significantly larger number of grid nodes (i.e., smaller spacing between grid nodes) required for the OPENFOAM simulations compared to the spectral simulations.

IV. SIMULATION RESULTS

A detailed comparison of the velocity and temperature fields obtained from the DNS and LES [17,18] has been performed. The results show quantitative and qualitative agreement. Therefore, to avoid unnecessary repetition, we will primarily exhibit DNS results unless otherwise stated. Here, in order to give an overall impression of the flow, we present results for the temporal evolution of the Nusselt number, the relation between the Nusselt and Rayleigh numbers, visualizations of instantaneous snapshots of the temperature and index of refraction fields, and the statistics associated with these fields.

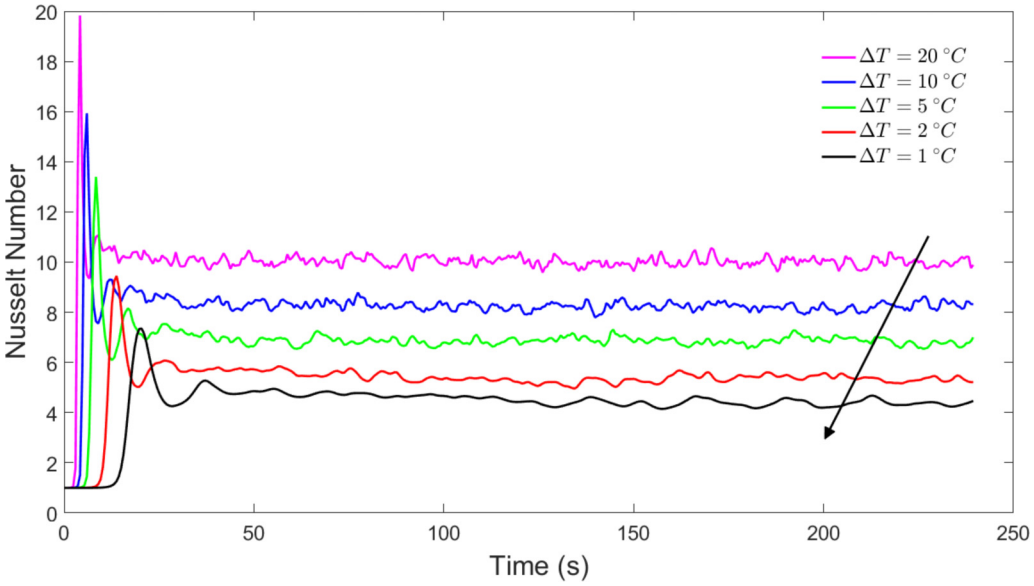

FIG. 1. Nusselt number ($\mathrm{Nu} = QL/k\Delta T$) versus time obtained from the DNS. Arrow indicates decreasing ΔT.

A. Temporal evolution of the Nusselt number

The evolution of the Nusselt number, which is essentially a proxy for the heat flux across the domain, is shown in Fig. 1 for all DNS runs. Since the Rayleigh number for all runs was above the linear stability limit, flow instability was induced by seeding the initial velocity field with small random values. This excites a strong response, as can be seen by the rapid increase of the Nusselt number in the first few seconds of each simulation. The flows are seen to fairly quickly establish a steady state in which the Nusselt number oscillates randomly about a mean value. All statistics from the DNS runs were obtained by averaging over the last 60 s of these simulations.

B. Visualization of the temperature field

In Fig. 2, a three-dimensional snapshot of the instantaneous temperature field obtained from the last 60 s of the DNS for $\Delta T = 20\,^\circ\mathrm{C}$ and $\mathrm{Ra} = 2.126\times10^6$ is shown. The numerous warm (red) and cold (blue) cusplike shapes at the bottom and top walls correspond to rising and falling fluid respectively, which was confirmed through numerous visualizations of the velocity field not shown here.

C. Dependence of the Nusselt number on Rayleigh number

In Fig. 3 the dependence of the Nusselt number on the Rayleigh number is shown for both DNS and LES. The results show close agreement over a range of more than one order of magnitude in Rayleigh number, despite the significant differences between the two numerical approaches. In addition, a least squares curve fit using the data from both simulations gives $\mathrm{Nu} = 0.186\mathrm{Ra}^{0.274}$. This is in reasonable agreement with $\mathrm{Nu} = 0.1\mathrm{Ra}^{0.31}\mathrm{Pr}^{0.05}$ obtained from a series of comprehensive experiments [19] cited in the classic work of Chandrasekar in 1961 [9] as representative of laboratory scale RB turbulence. However, it is important to recognize that the relationship between the Nusselt, Rayleigh, and Prandtl numbers for RB turbulence will be sensitive to the aspect ratio (L/L_x) as well as the boundary conditions employed on the side walls.

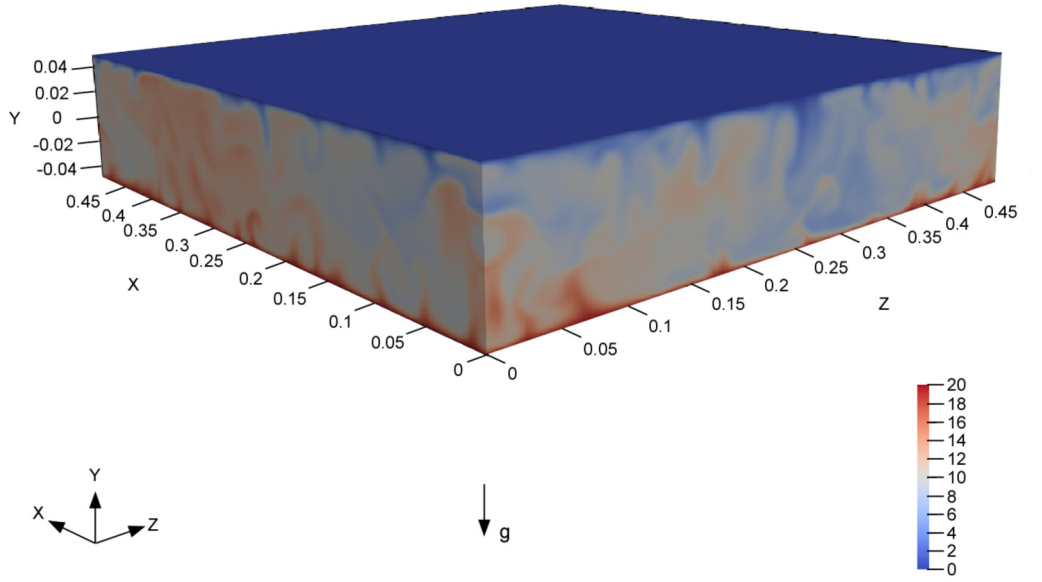

FIG. 2. Three-dimensional visualization of the temperature field, $\theta = T - T_0$(°C), obtained from a statistically steady state flow from the DNS for which $\Delta T = 20\,^{\circ}$C and Ra $= 2.126\times10^6$ at $t = 180$ s. Hot and cold fluid associated with cusplike regions are rising and falling from bottom and top boundaries respectively. Axes are denoted in meters and the arrow indicates the direction of gravity.

D. Visualization of the index of refraction field

We are concerned with the index of refraction in this work, since its structure function can be used to determine the structure function constant C_n^2. It is straightforward to determine the index of

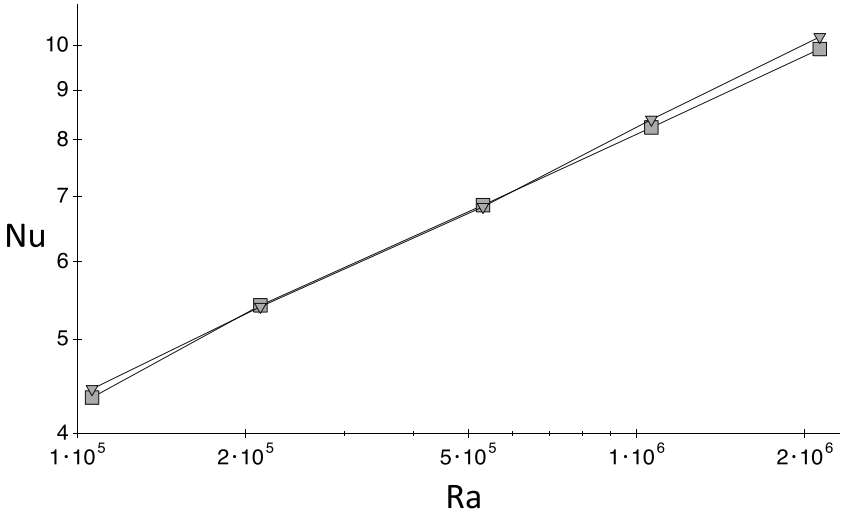

FIG. 3. Nusselt number vs Rayleigh number. DNS: ■ LES: ▼. The Nusselt number was obtained from the heat flux at the top and bottom walls of the domain during a time period in which the flow was statistically steady. A least squares curve fit of these results gives $\mathrm{Nu} = 0.186\mathrm{Ra}^{0.274}$.

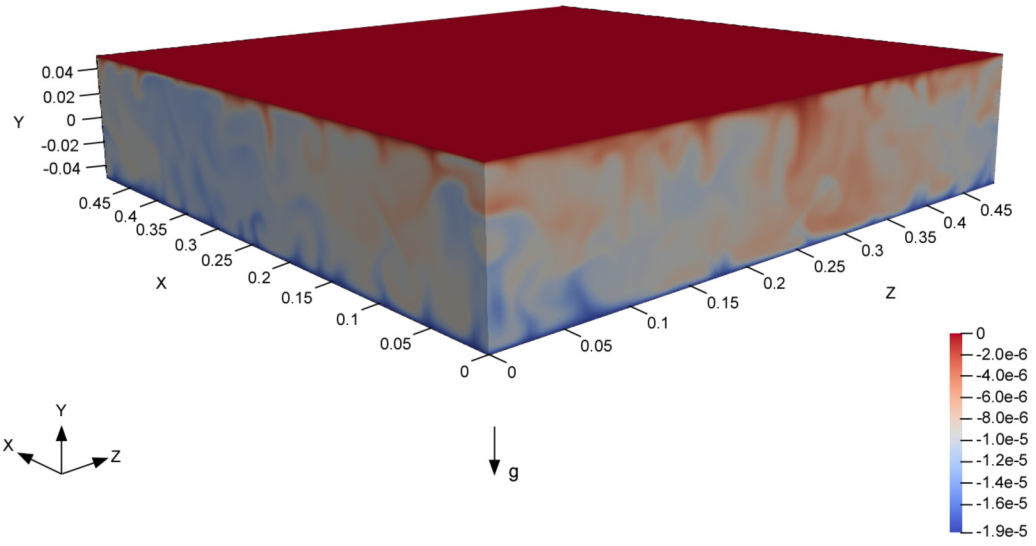

FIG. 4. Three-dimensional snapshot of the index of refraction field, $n_0 = n-1$. This image was generated from the thermal field shown in Fig. 2.

refraction n in air from the temperature field as follows [1]:

$$n - 1 = -C\frac{p_0}{T_0^2}(T - T_0), \tag{4}$$

where $C = 79\times10^{-6}$ K/mbar, $p_0 = 1013.25$ mbar, and T_0 is the reference temperature. The left-hand side represents deviations of the index of refraction from its equilibrium value of 1. In Fig. 4 a three-dimensional snapshot of $n_0 = n-1$ is shown. Here it is evident that n_0 is strictly negative since the temperature field is always greater than the reference temperature, which is defined to be the temperature of the top wall. Rising warm plumes (see Fig. 2) are seen to be associated with the largest negative index of refraction (e.g., blue cusplike features in Fig. 4).

In Figs. 5(a) and 5(b) horizontal (x–z) slices of the index of refraction field, obtained from the Fig. 4 snapshot, are shown. Figure 5(a) shows that the index of refraction field near the top wall exhibits an interesting *spider-web* structure composed of narrow (red) linear features. These features have been confirmed to be associated with falling cold plumes. On the other hand, the index of refraction field at the exact center of the flow shown in Fig. 5(b) appears relatively featureless.

E. Statistics of the temperature, velocity, and index of refraction

The statistics of the temperature, velocity, and index of refraction fields are presented in Figs. 6–8. Here for any field ϕ, $\bar{\phi}$ is defined as its average (mean) and is obtained by summing over all realizations of the flow in a given time period and over the horizontal plane. Its root-mean-square (rms) is defined by $\phi_{\rm rms}(y) = [\overline{(\phi-\bar{\phi})^2}]^{1/2}$. All statistics presented here were obtained over the time interval t = 180–240 s for each simulation. It is expected that the so-called *convective scales* [20] of velocity, w^*, and temperature, θ^*, defined by

$$w^* = (\beta g L q_0)^{1/3} \tag{5}$$

and

$$\theta^* = q_0/w^* \tag{6}$$

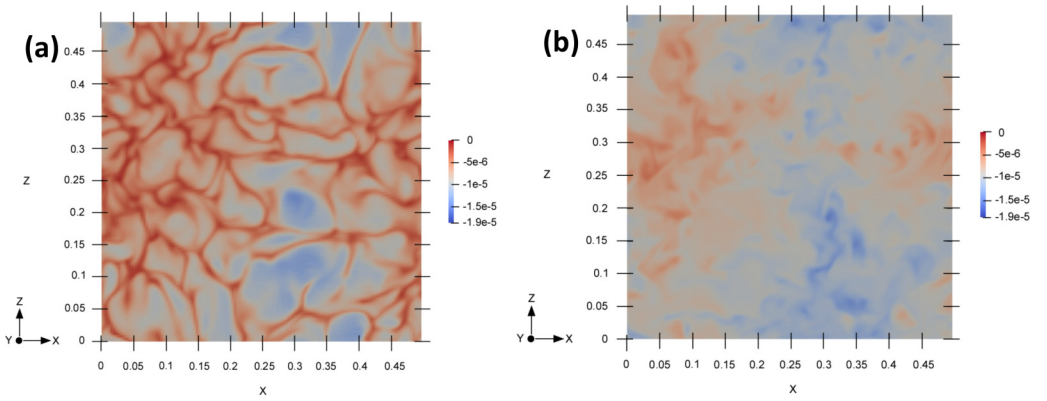

FIG. 5. (a) Visualization of the index of refraction field, $n_0 = n-1$, in the horizontal ($x-z$) plane near the top surface ($y = 0.045$ m) obtained from the snapshot shown in Fig. 4. Note the spider-web-like structure. (b) Visualization of the index of refraction field in the horizontal ($x-z$) plane at the center ($y = 0.0$ m) of the domain.

give reasonable estimates of the velocity and thermal fluctuations for RB turbulence, where $q_0 = Q/(\rho c_p)$, and Q is the heat flux.

The mean temperature profiles shown in Fig. 6(a) indicate the expected deviations from the linear conduction profile used as the initial condition in each simulation as turbulent mixing increases thermal gradients near the walls. As an example, the heat flux for the case $\Delta T = 20\,^{\circ}$C has increased by about one order of magnitude compared to pure thermal conduction as indicated by the fact that the Nusselt is $\mathcal{O}(10)$ in this case, as shown in Fig. 3. The rms thermal profiles shown in Fig. 6(b) have been scaled using θ^*. This scaling appears to give good data collapse in the central region. Further, the thermal fluctuations scaled in this way are all $\mathcal{O}(1)$, which confirms that the thermal convective scale gives reasonable estimates of thermal fluctuation magnitudes. The rms velocity profiles shown in Fig. 7 have been scaled using w^*. Similar to the thermal fluctuations, all three velocity components are $\mathcal{O}(1)$, and the horizontal (u, w) velocity results show that the flow has no $x-z$ bias as we should expect from the symmetry of the flow.

In the center of the flow, although the vertical (v) fluctuations are somewhat larger than the horizontal (u, w) fluctuations, it is reasonable to assume that the flow can be considered nearly isotropic at its center. In fact, this was also found to be true in recent experiments [21]. Finally, the

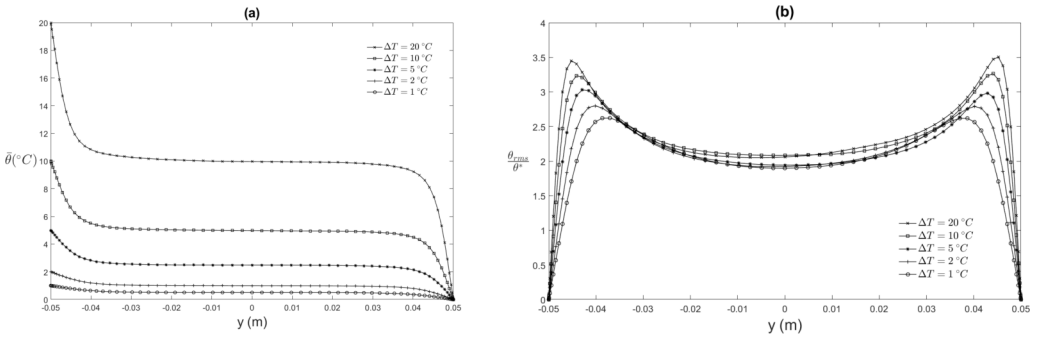

FIG. 6. Temperature statistics obtained from the DNS. (a) Mean temperature $\bar{\theta}$ versus vertical distance y for five temperature differences ΔT. The bottom wall of the domain is at $y = -0.05$ m. (b) Root-mean-square temperature $\theta_{\rm rms}$ made nondimensional by the convective thermal scale θ^*.

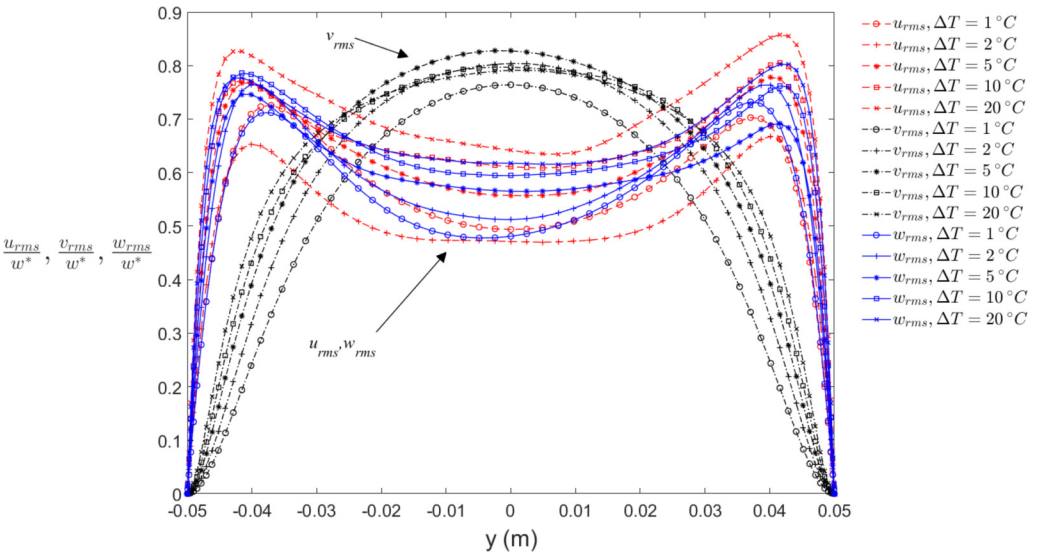

FIG. 7. Root-mean-square velocities, $u_{\rm rms}$, $v_{\rm rms}$, $w_{\rm rms}$, obtained from the DNS. These have been made nondimensional by the convective velocity scale w^*.

rms of the index of refraction fluctuations ($\eta_{\rm rms}$) are shown in Fig. 8(a). We note that these profiles, along with those for the horizontal (u, w) velocity components and those for temperature fields, all exhibit maxima near the no-slip walls, where the turbulence is expected to deviate from isotropy. In addition, as shown in Fig. 8(b), when $\eta_{\rm rms}$ is scaled with the characteristic convective temperature scale θ^*, we see that reasonable collapse is obtained. This is expected since from Eq. (4), index of refraction fluctuations are proportional to thermal fluctuations.

V. MODEL FOR THE STRUCTURE FUNCTION CONSTANTS

In RB turbulence, it is appropriate to define the structure function for temperature fluctuations as a function of r, which represents a coordinate in a given horizontal (x−z) plane, and the coordinate y, which corresponds to that plane as follows:

$$D_T(r, y) = \langle [T(0, y) - T(r, y)]^2 \rangle, \tag{7}$$

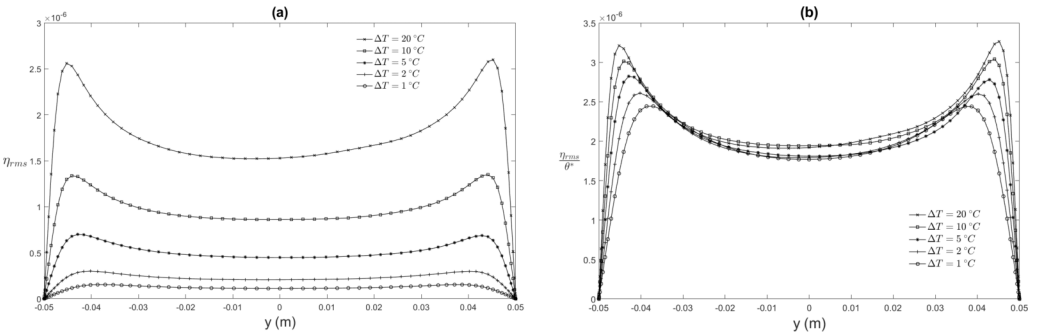

FIG. 8. (a) Root-mean-square index of refraction, $\eta_{\rm rms}$, and (b) $\eta_{\rm rms}/\theta^*$. These results were obtained from the DNS.

where the brackets represent averaging over all flow realizations. According to Kolmogorov scaling laws [22] there exists a region such that $l_0 \ll r \ll L_0$, the so-called inertial region, where l_0 and L_0 are the inner and outer scales of turbulence for which the structure function is

$$D_T(r, y) = C_T^2 r^{2/3}, \tag{8}$$

where C_T^2 is the structure function constant for thermal fluctuations. Similarly, the structure function D_n for the index of refraction fluctuations is defined by

$$D_n(r, y) = \langle [n(0, y) - n(r, y)]^2 \rangle. \tag{9}$$

Since the index of refraction fluctuations are assumed to be directly proportional to thermal fluctuations, as a first approximation [1] we must have

$$D_n(r, y) = K^2 C_T^2 r^{2/3}, \tag{10}$$

where $K = -C\frac{p_0}{T_0^2}$, so that an estimate C_T^2 will allow us to estimate C_n^2 as follows:

$$C_n^2 = K^2 C_T^2. \tag{11}$$

The proposed model for the structure function constants is based on data obtained from the exact center of the simulated RB turbulence where we have shown above that the turbulence is reasonably close to isotropy. Therefore C_T^2 can be directly related to the properties of an isotropic, homogeneous turbulence in the inertial range [22] by

$$C_T^2 \sim \epsilon_T \epsilon^{-1/3}, \tag{12}$$

where $\epsilon_T = \alpha \langle \partial_i T' \partial_i T' \rangle$ is the rate of dissipation of temperature fluctuations, $\epsilon = 2\nu \langle S_{ij} S_{ij} \rangle$ is the rate of dissipation of kinetic energy, $S_{ij} = 1/2(\partial_j u_i + \partial_i u_j)$ is the rate-of-strain tensor, fluctuations in temperature and velocity are given by T' and u_i, and repeated indices imply summation. Furthermore, since the simulated RB turbulence is in a statistically steady state, the production of turbulence equals the rate at which it is being dissipated. In this case, energy is assumed to be supplied to the turbulence at the largest length scales and is dissipated in one large-eddy turnover time, $t_E = L/w^*$, a basic assumption in the Kolmogorov model of turbulence [22]. These considerations lead to the following estimates for the dissipation rates in terms of the convective scales $w^*$and θ^* and the t_E:

$$\epsilon_T \sim (\theta^*)^2 w^*/L, \tag{13}$$

and

$$\epsilon \sim (w^*)^3/L. \tag{14}$$

The final estimate for C_T^2 can be determined by substituting Eqs. (13) and (14) into Eq. (12) which gives

$$C_T^2 \sim \left(\frac{Q}{\rho c_p L}\right)^{4/3} (\beta g)^{-2/3}. \tag{15}$$

This result implies that

$$C_T^2/\chi \equiv \gamma, \tag{16}$$

where $\chi = (\frac{q_0}{L})^{4/3}(\beta g)^{-2/3}$ and γ is a dimensionless constant which should not depend on Rayleigh or Prandtl numbers. Naturally, since the Rayleigh number depends on the Nusselt and Prandtl numbers, γ should also be independent of the Nusselt number as well. The extent to which this model describes the nature of the structure function constant will be determined by comparing it to simulations.

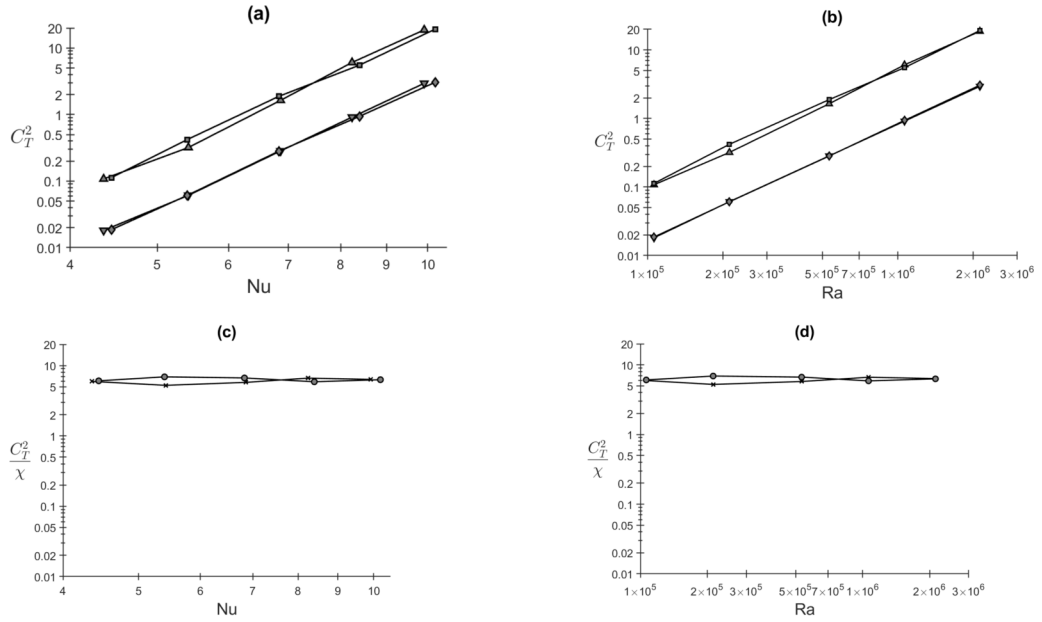

FIG. 9. Dependence of thermal structure function constant C_T^2 on the Nusselt number (a) and Rayleigh number (b). Theory given by $C_T^2 = (\frac{Q}{\rho c_p L})^{4/3}(\beta g)^{-2/3}$ using the Q from DNS (▼) and LES (◆). C_T^2 from DNS (▲) and LES (■). Dependence of the thermal structure function constant made nondimensional by the theory (C_T^2/χ) on Nusselt number (c) and Rayleigh number (d) for DNS (×) and LES (●). Dimensions of C_T^2 are $^\circ\mathrm{C}^2\mathrm{m}^{-2/3}$.

VI. COMPARISON OF THE MODEL FOR C_T^2 AND C_n^2 WITH SIMULATIONS

For both the DNS and LES simulations, the structure function D_T was determined using Eq. (7) and data from the center plane of the computational domain. Then using Eq. (8), the best fit of the structure function to the two-thirds law was used to determine the structure function constant C_T^2. In all cases, the goodness of fit parameter R^2 was greater than 0.95 indicating that the two-thirds law was well satisfied.

In Figs. 9(a) and 9(b) the dependence of C_T^2 on Nusselt and Rayleigh numbers are shown for both DNS and LES simulations. These results are compared with the theory given by Eq. (15). It is evident that the simulation results and the theory show the same dependence on Nusselt and Rayleigh numbers since both simulation and theory give nearly straight lines with virtually the same slopes as shown using log-log axes. Furthermore, when C_T^2 is made nondimensional as described in Eq. (16), it is clear from Figs. 9(c) and 9(d) that γ is essentially independent of the Nusselt and Rayleigh numbers, as predicted by the theory.

Naturally, we expect some variation in the constant γ. Using the DNS and LES data, the average and root-mean-square values for γ are found to be $\bar{\gamma} = 6.171$ and $\gamma_{\mathrm{rms}} = 0.4721$ respectively. The final result for the normalized thermal structure function constant for RB turbulence is then

$$C_T^2/\chi = 6.171 \pm 0.4721. \tag{17}$$

The dependence of the index of refraction constant C_n^2 on heat flux is shown in Fig. 10. Here the theory, given by $C_n^2 = \bar{\gamma} K^2 (\frac{Q}{\rho c_p L})^{4/3}(\beta g)^{-2/3}$, is compared to the simulations. Excellent agreement is obtained, confirming that the model given by Eq. (15) gives an accurate estimate of the index of refraction structure function constant. We note that although we have shown that C_T^2/χ is independent of the Nusselt and Rayleigh numbers, we have not shown that it is independent of the

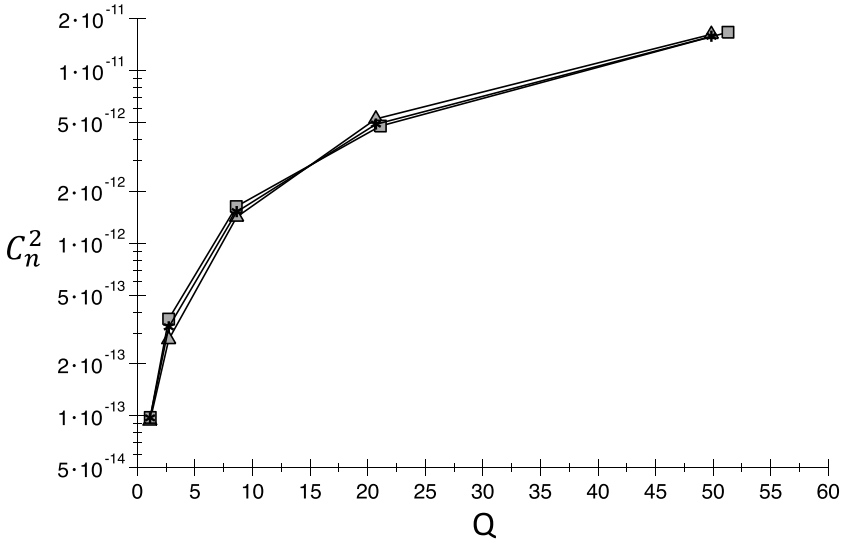

FIG. 10. Dependence of the index of refraction structure function constant, $C_n^2 = K^2 C_T^2$ where $K = -C\frac{p_0}{T_0^2}$, on heat flux Q (W/m^2). Simulation results: DNS (▲), LES (■). Theory (∗) given by $C_n^2 = \bar{\gamma} K^2 (\frac{Q}{\rho c_p L})^{4/3} (\beta g)^{-2/3}$. Units for C_n^2 are m$^{-2/3}$.

Prandtl number. This dependence, if any, could not be determined based on our current simulations which were performed at constant Prandtl number.

VII. SUMMARY AND DISCUSSION

The objective of this effort was to determine the efficacy of determining the properties of optical turbulence through the use of three-dimensional numerical simulations. The classic and well-studied case of Rayleigh-Bénard turbulence was chosen for the simulations since this form of turbulence has many of the features we expect to find in natural flows in atmospheres and oceans, and is therefore of particular interest to the optics and fluid mechanics communities. The simulations were used to study the nature of the structure function constant C_n^2. This statistic is a measure of the intensity of optical turbulence, and therefore determines the effects of thermal fluctuations on the propagation of light through random media.

The simulations were carried out for air using two different numerical schemes: (A) Pseudospectral methods using an in-house code (DNS), and (B) A finite-volume method which employs a large-eddy-simulation (LES) model using the OPENFOAM toolbox. The DNS and LES were carried out in identically the same computational domain (aspect ratio of 5:1), with identically the same fluid properties, and for the same temperature changes across the domain ($\Delta T = 1\,^\circ$C, $2\,^\circ$C, $5\,^\circ$C, $20\,^\circ$C). This resulted in a Rayleigh number variation of 1.063×10^5 to 2.126×10^6. The statistics (e.g., velocity, temperature) obtained from the DNS and LES simulations were compared in previous work, and were shown to be in very close agreement. It is important to emphasize that such close agreement was obtained despite the fact that the DNS and LES use different representations for the small scales of turbulence, and were performed on entirely different computational platforms. In fact, the DNS uses no turbulence models, and therefore uses no special representation of the smallest scales of turbulence.

Three-dimensional visualizations of the temperature and index of refraction fields show a dendritic or spider-web structure near the walls, and a more featureless structure at the center of the domain. Root-mean-square (rms) statistics of the velocity field reveal an isotropic structure at

the domain center, and are shown to collapse reasonably well by using the convective scale w^*. Similarly, the rms statistics of the temperature field are shown to collapse using the scale θ^*.

A model for the structure function constant for RB turbulence is proposed based on the idea that the turbulence is nearly isotropic at its center, which allows the standard Kolmogorov theory of turbulence to be invoked. Based on this idea, the structure function constant for the thermal fluctuations C_T^2 can be represented in the inertial range by $C_T^2 \sim \epsilon_T \epsilon^{-1/3}$, where ϵ_T and ϵ are the dissipation rates for the temperature and kinetic energy respectively. The dissipation rates as well as the large eddy turnover time can then be expressed in terms of the convective scales to give $C_T^2/[(\frac{q_0}{L})^{4/3}(\beta g)^{-2/3}] \equiv \gamma$, where γ is a constant, independent of Rayleigh or Prandtl numbers. Excellent agreement was found between this theoretical result and the simulations. The comparison gives the final result of this work: $C_T^2/\chi = 6.171 \pm 0.4721$. From this, C_n^2 can be determined since it is directly proportional to C_T^2. We emphasize that the theory predicts that γ should be independent of Rayleigh number, which is confirmed by the simulations for a one order of magnitude change in the Rayleigh number.

In conclusion, this work shows the efficacy in using numerical simulations to obtain important properties of optical turbulence, as well as a means of verifying theoretical estimates of these properties. We also recognize the importance of experimentally verifying the results obtained in this work. In particular, the theory predicts that the structure function constant is related to the heat flux Q as follows: $C_T^2 \sim Q^{4/3}$. An experimental effort with this goal in mind is now underway in the Clemson University VTG (Variable Turbulence Generator) facility [23,24].

The data that support the findings of this study are available from the corresponding author upon reasonable request.

ACKNOWLEDGMENTS

R.A.H. and R.J.W. acknowledge funding provided by ONR MURI Grant No. N00014-20-1–2558 and the generous allotment of computer time on the Clemson University Palmetto cluster. This work was also supported in part by an NRL base program. Numerical simulations with OPENFOAM were performed on resources provided by the DoD Supercomputing Resource Center (ARL DSRC).

[1] L. C. Andrews and R. L. Phillips, *Laser Beam Propagation Through Random Media* (SPIE, Bellingham, Washington, 2005).

[2] R. Frehlich, R. Sharman, F. Vandenberghe, W. Yu, Y. Liu, J. Knievel, and G. Jumper, Estimates of C_n^2 from numerical weather prediction model output and comparison with thermosonde data, J. Appl. Meteor. Climatol. **49**, 1742 (2010).

[3] V. I. Tatarskii, *The Effects of the Turbulent Atmosphere on Wave Propagation* (Israel Program for Scientific Translations, Jerusalem, 1971).

[4] M. Azouit and J. Vernin, Optical turbulence profiling with balloons relevant to astronomy and atmospheric physics, Publ. Astron. Soc. Pac. **117**, 536 (2005).

[5] H. A. Panofsky, The structure constant for the index of refraction in relation to the gradient of index of refraction in the surface layer, J. Geophys. Res. **73**, 6047 (1968).

[6] W. Hou, S. Woods, E. Jarosz, W. Goode, and A. Weidemann, Optical turbulence on underwater image degradation in natural environments, Appl. Opt. **51**, 2678 (2012).

[7] D. Lohse and K. Q. Xia, Small-scale properties of turbulent Rayleigh-Bénard convection, Annu. Rev. Fluid Mech. **42**, 335 (2010).

[8] L. Rayleigh O. M. F. R. S., LIX. On convection currents in a horizontal layer of fluid, when the higher temperature is on the under side, Philos. Mag. (1798–1977) **32**, 529 (1916).

[9] S. Chandrasekhar, *Hydrodynamic and Hydromagnetic Stability* (Oxford University Press, 1961).

[10] D. L. Fried, Optical resolution through a randomly inhomogeneous medium for very long and very short exposures, J. Opt. Soc. Am. B **56**, 1372 (1966).
[11] J. M. Mihaljan, A rigorous exposition of the boussinesq approximations applicable to a thin layer of fluid, Astrophys. J. **136**, 1126 (1962).
[12] K. Morris, R. A. Handler, and D. W. I. Rouson, Intermittency in the turbulent Ekman layer, J. Turbul. **12**, N12 (2011).
[13] F. Nicoud and F. Ducros, Subgrid-scale stress modelling based on the square of the velocity gradient tensor, Flow Turbul. Combust. **62**, 183 (1999).
[14] P. J. Roach, *Computational Fluid Dynamics* (Hermosa, Albuquerque, 1972).
[15] C. Canuto, M. Y. Hussaini, A. Quarteroni, and T. A. Zang, *Spectral Methods in Fluid Dynamics* (Springer-Verlag, Berlin, 1987).
[16] R. Sureshkumar, A. N. Beris, and R. A. Handler, Direct numerical simulation of the turbulent channel flow of a polymer solution, Phys. Fluids **9**, 743 (1997).
[17] K. P. Judd, S. Avramov-Zamurovic, S. Matt, R. A. Handler, A. T. Watnik, J. R. Lindle, J. Esposito, and W. A. Jarrett, Propagation of laser beams carrying orbital angular momentum through simulated optical turbulence, in *Rayleigh-Bénard Convection, Environmental Effects on Light Propagation and Adaptive Systems IV*, SPIE Remote Sensing International Symposium Vol. 11860 (SPIE, Bellingham, Washington, 2021), pp. 20–32.
[18] S. Matt, K. P. Judd, S. Avramov-Zamurovic, A. T. Watnik, and R. A. Handler, Numerical representation of Rayleigh-Bénard convection for the study of optical propagation through turbulence, Proc. SPIE **12118**, 121180B (2022).
[19] P. L. Silveston, Warmedurchgang in waagerechten Flussigkeitsschichten, Forsch. Geb. Ingenieurwes. **24**, 59 (1958).
[20] R. J. Adrian, R. T. D. S. Ferreira, and T. Boberg, Turbulent thermal convection in wide horizontal fluid layers, Exp. Fluids **4**, 121 (1986).
[21] R. Ni, S. Huang, and K. Xia, Local energy dissipation rate balances local heat flux in the center of turbulent thermal convection, Phys. Rev. Lett. **107**, 174503 (2011).
[22] H. Tennekes and J. L. Lumley, *A First Course in Turbulence* (MIT Press, Cambridge, MA, 1972).
[23] R. J. Watkins, K. Dai, G. White, W. Li, J. K. Miller, K. S. Morgan, and E. G. Johnson, Experimental probing of turbulence using a continuous spectrum of asymmetric OAM beams, Opt. Express **28**, 924 (2020).
[24] M. Lemon, E. Robertson, J. Free, K. Dai, J. K. Miller, L. Vanderschaaf, M. Cox, R. J. Watkins, and E. G. Johnson, Sensing and coupling of optical channels in dynamic atmospheric turbulence using OAM beamlets for improved power and data transmission, Opt. Express **30**, 47598 (2022).